Research Square

Preprints are preliminary reports that have not undergone peer review.
They should not be considered conclusive, used to inform clinical practice,
or referenced by the media as validated information.

Ligand-Engineered Cu-MOF Nanozyme-Based Triple-Channel Colorimetric Sensor Array with Machine Learning for Rapid Discrimination of Aminoglycoside Antibiotics

Zhiyuan Luo
Chongqing University of Technology
Ziyi Zhao
Chongqing University of Technology
Hailong Shi
Chongqing University of Technology
Lingyun Cheng
Chongqing University of Technology
Miao Zhang
Chongqing University of Technology
Haixia Feng
Chongqing University of Science and Technology
Yuwan Lu
2024054@cqust.edu.cn

Chongqing University of Science and Technology
Siqi Li
Chongqing University of Technology

Research Article

Keywords: Cu-MOFs, sensor arrays, colorimetric, aminoglycoside antibiotics, machine learning

Posted Date: November 23rd, 2026

DOI: https://doi.org/10.21203/rs.3.rs-11621777/v1

License: This work is licensed under a Creative Commons Attribution 4.0 International License.
Read Full License

Additional Declarations: No competing interests reported.

Ligand-Engineered Cu-MOF Nanozyme-Based Triple-Channel Colorimetric Sensor Array with Machine Learning for Rapid Discrimination of Aminoglycoside Antibiotics

Zhiyuan Luo[a], Ziyi Zhao[a], Hailong Shi[a], Lingyun Cheng[a], Miao Zhang[a], Haixia Feng[b], Yuwan Lu[b,*], Siqi Li[a,*]

[a]School of Pharmacy and Bioengineering, Chongqing University of Technology, Chongqing 400054, PR China

[b]School of Chemistry and Chemical Engineering, Chongqing University of Science and Technology, Chongqing, 401331, PR China

*Corresponding author

E-mail address: lisiqi47@cqut.edu.cn (Siqi Li);

E-mail address: 2024054@cqust.edu.cn (Yuwan Lu);

Abstract

The structural similarity of aminoglycoside antibiotics (AGs) poses a critical challenge for their simultaneous detection and differentiation. To address this, we report a three-channel colorimetric sensor array based on ligand-engineered metal-organic frameworks (Cu-MOFs) for rapid discrimination of five AGs (amikacin, gentamicin, tobramycin, streptomycin, and kanamycin). By modulating the organic ligands, three Cu-MOFs (Cu-TPA(NO_2), Cu-TPA(NH_2), and Cu-IPA) with distinct peroxidase-like activity toward peroxymonosulfate (PMS) activation were screened under neutral conditions, which enables ultrafast activation of the chromogenic reaction and overcomes the prolonged incubation times typically required in conventional nanozyme-based assays. Each AG differentially modulates the PMS activation behavior of the three Cu-MOFs, producing characteristic absorbance changes at 418 nm that serve as unique fingerprint responses. Coupled with linear discriminant analysis and hierarchical clustering analysis, the array enables qualitative identification and quantitative analysis of the five AGs within 5 min over a linear range of 1-10 μg/mL, with a limit of detection down to 0.5 μg/mL. The sensor array also successfully distinguishes binary and ternary AG mixtures, and its practical utility is validated by accurate classification of commercial gentamicin formulations. This PMS-enabled rapid catalytic strategy offers a simple and robust tool for on-site screening of aminoglycoside residues in complex samples, representing a previously unexplored approach for AGs sensor array construction.

Keywords: Cu-MOFs; sensor arrays; colorimetric; aminoglycoside antibiotics; machine learning

Introduction

Aminoglycoside antibiotics (AGs), characterized by two or more amino sugars linked to a 2-deoxystreTPAmine ring via glycosidic bonds, constitute a class of broad-spectrum antibacterial agents widely employed in clinical therapy and veterinary medicine owing to their potent efficacy and cost-effectiveness[1, 2]. However, their clinical utility is severely constrained by intrinsic adverse effects, including ototoxicity and nephrotoxicity[3, 4]. Moreover, the environmental persistence of AGs not only poses risks of chemical toxicity and allergic sensitization but also accelerates the dissemination of antibiotic resistance genes, thereby threatening public health[5, 6]. Consequently, the development of rapid, reliable, and cost-effective analytical methods for AGs detection is of paramount importance.

Conventional analytical techniques, including microbiological methods[7], immunoassays[8], high-performance liquid chromatography[9], and fluorescence detection methods[10], offer satisfactory sensitivity and accuracy but are invariably constrained by expensive instrumentation, labor-intensive sample pretreatment, and the need for skilled operators. Colorimetric methods[11] have emerged as attractive alternatives owing to their operational simplicity, low cost, naked-eye readability, and rapid response, making them particularly suitable for high-throughput screening and point-of-use applications[4, 12]. In recent years, sensor arrays-often referred to as “chemical tongues” or “electronic noses”-have garnered considerable interest by mimicking the mammalian olfactory system through cross-reactive sensing elements. The sensor array consists of multiple sensing units with cross-responses [13]. Each unit exhibits a distinct response intensity to different analytes, and the same target substance generates distinguishable recognition signals across different units[14, 15]. By integrating and analyzing the multi-channel output signals, the array can establish a unique response fingerprint for each analyte, thereby enabling the effective differentiation of various similar components in complex matrices[16]. This technology has emerged as a promising tool for identifying a wide range of analytes in fields such as environmental monitoring, [17, 18] food safety, [19, 20] and disease diagnosis, [21-

23], where it has made significant progress in the precise identification and detection of antibiotics. For example, Chen's team developed a partitioned dual-nanocase cascade complex (Au@mPDA/PAACu_2MI, AMPC) for the colorimetric detection of AGs and conducted a detailed analysis of the catalytic mechanism of this dual-enzyme system [4]. Li et al. developed a machine learning-based colorimetric sensor array that successfully achieved both qualitative and quantitative analysis of AGs[11]. Despite these advances, most reported AGs sensor arrays rely on a single nanozyme material with limited differential response channels, resulting in insufficient signal diversity and prolonged incubation times. More critically, the concentration-dependent nature of these responses often leads to misclassification, as a high concentration of one analyte may produce a pattern akin to that of a lower concentration of another. These limitations severely impede the reliable discrimination of structurally analogous AGs in real-world scenarios, where both identity and concentration are unknown.

Metal-organic frameworks (MOFs) offer unique advantages in optical sensing and nanozyme catalysis due to their highly tunable structures, large specific surface areas, and abundant active sites. Notably, ligand engineering provides a versatile strategy to modulate the coordination microenvironment of metal nodes, thereby tailoring the catalytic activity and substrate selectivity of MOF nanozymes. MOFs constructed with distinct organic linkers exhibit diverse surface properties, pore structures, and host–guest interaction capabilities, allowing them to interact uniquely with various analytes through multiple mechanisms, including electrostatic interactions, π-π stacking, hydrogen bonding, and coordination [24, 25]. This ligand-dependent multifunctionality positions MOFs as promising building blocks for sensor arrays, where each MOF variant serves as a distinct sensing channel to generate cross-reactive response fingerprints toward multiple targets. Simultaneously, machine learning has emerged as a powerful data-processing tool that excels in cluster analysis, classification, and regression, and is increasingly integrated with sensor arrays to enhance recognition accuracy and overcome concentration-induced misclassification [26]. Several representative machine learning algorithms, such as linear discriminant analysis, hierarchical clustering, k-nearest neighbors, and artificial neural networks, have been

integrated with sensor arrays for multi-target recognition [27].

Inspired by these considerations, we herein develop a ligand-microenvironment-engineered Cu-MOF-based triple-channel colorimetric sensor array, synergistically coupled with machine learning, for the rapid and accurate discrimination of five AGs (**Scheme 1**). Three Cu-MOFs (Cu-TAP(NO_2), Cu-TAP(NH_2), and Cu-IPA) with distinct PMS activation efficiencies are synthesized by simple ligand modulation. The Cu-MOFs catalyze the activation of PMS, generating various ROS that further oxidize the substrate ABTS, leading to a color chang. The differential responses of these three Cu-MOFs-PMS-ABTS sensing units toward each AG generate unique absorbance fingerprints, while linear discriminant analysis (LDA) and hierarchical clustering analysis (HCA) enable both qualitative identification and quantitative analysis of KAN, AMK, TOB, GMC, and STR. Furthermore, the sensor's anti-interference capability and real-world applicability were systematically evaluated using representative interfering compounds and commercial pharmaceutical formulations, respectively. This work establishes a new paradigm for ligand-regulated MOF nanozyme sensor arrays, offering a simple, rapid, and intelligent platform for antibiotic screening with potential extension to other classes of environmental pollutants.

Scheme 1

Experimental

Synthesis of Cu-MOFs

The preparation of Cu-MOFs followed the method previously reported [28]. Briefly, 2.21 mmol of TPA-NO_2 was dissolved in 20 mL of a 1:1 mixture of DMF and ethanol. 4.14 mmol of $Cu(NO_3)_2 \cdot 3H_2O$ was dissolved in 10 mL of deionized water. Next, the mixed solution was transferred to a high-pressure reactor and reacted at 85 ^oC for 24 h. The product was collected after centrifugation, washing, and drying. A similar synthesis procedure was then carried out, with the exception that TPA-NO_2 was replaced by TPA-NH_2, TPA, IPA-NH_2, and IPA, while all other conditions remained unchanged. The resulting products were Cu-TPA(NH_2), Cu-TPA(NO_2), Cu-TPA, Cu-IPA(NH_2), and Cu-IPA, respectively.

Performance of Cu-MOFs in the Catalytic Activation of PMS

The catalytic activity of materials such as Cu-TPA(NO_2), Cu-TPA(NH_2), Cu-IPA(NH_2), Cu-TPA, and Cu-IPA was investigated by catalyzing the oxidation reaction between peroxymonosulfate (PMS) and 2,2'-bipyridyl-3-sulfonic acid ammonium salt (ABTS). 50 μL of Cu-MOFs (200 mg/L), 50 μL of ABTS (50 mM), and 10 μL of PMS (10 mM) were added to Tris-HCl buffer (10 mM, pH 7.4) to give a final reaction volume of 1 mL. After allowing the solution to react at room temperature for 10 min, the absorption spectrum of the solution was measured at wavelengths ranging from 400 to 800 nm using a UV-Vis spectrophotometer.

Developing a colorimetric sensor array for AGs identification

Solutions of various antibiotics (KAN, AMK, TOB, GMC, STR) at a concentration of 1 mg/mL were prepared for subsequent colorimetric sensor array recognition experiments. To each of the three channels of the sensor array, 100 μL of different Cu-MOFs (Cu-TPA(NO_2), Cu-TPA(NH_2), Cu-IPA), 50 μL of ABTS (50 mM) solution, 5 μL (10 mM) of PMS solution, 845 μL of Tris-HCl buffer (pH 7.4), and 10 μL of the respective antibiotic solution. The reaction was allowed to proceed at room temperature (25 ^oC) for 5 min. The absorbance of each channel at 418 nm was measured using UV-Vis spectrophotometry. The measured absorbance was designated as A, while the blank

signal was recorded as A_0. The response signal was calculated as $(A_0\text{-}A)/A_0$. LDA and HCA were performed on the response signals of the three channels using SPSS statistical software. The analysis was performed on the response matrix comprising 3 sensing channels × 5 antibiotics × 5 replicates. A series of antioxidant solutions with varying concentration gradients (1-50 μg/mL) was prepared to facilitate the subsequent differentiation and quantification of antioxidants at different concentrations. Following the experimental protocol described above, each antioxidant solution at different concentrations was introduced into the three separate channels, with a reaction time of 5 min. Subsequently, LDA and HCA analyses were performed on the response signals using SPSS statistical software.

Results and discussion

Characterization of Cu-MOFs

To enhance the catalytic activity of Cu-MOFs, we selected five ligands for the synthesis of Cu-MOFs. As shown in **Fig. 1a**, five types of Cu-MOFs were first synthesized by self-assembly via a conventional solvothermal reaction, using Cu^{2+} as the active center and five different organic ligands, respectively. The prepared materials were then comprehensively characterized using various techniques. As shown in **Fig. S1**, visual inspection reveals that the powders of the five Cu-MOFs have distinct colors. Scanning electron microscopy (SEM) reveals distinct morphology and particle size variations among the five Cu-MOFs. Specifically, Cu-TPA(NO_2) adopts a large flake-like morphology (**Fig. 1b**), whereas Cu-TPA(NH_2) forms agglomerated clusters (**Fig. 1c**). Cu-IPA(NH_2) also exhibits pronounced agglomeration (**Fig. S2a**), while Cu-TPA displays uniform rod-like particles (**Fig. S2b**), and Cu-IPA assumes a layered sheet structure (**Fig. 1d**). These results demonstrate that the size and morphology of Cu-MOFs are readily tunable simply by varying the organic ligand. Fourier transform infrared spectroscopy (FT-IR) revealed that the synthesized Cu-MOFs exhibited peaks corresponding to their respective ligands (**Fig. S3**).

The crystalline structures of the five Cu-MOFs were then further investigated.

Sharp characteristic diffraction peaks in the X-ray diffraction (XRD) patterns confirmed that all of them exhibit high crystallinity, and the positions of these peaks are consistent with those previously reported for Cu-MOFs (**Fig. S4**). These results confirm the successful synthesis of the five Cu-MOFs. X-ray photoelectron spectroscopy (XPS) was employed to investigate the elemental composition and chemical states of the five Cu-MOFs. The survey spectra confirmed the presence of C, O, and Cu in all samples, with additional N signals observed in Cu-TPA(NO_2), Cu-TPA(NH_2), and Cu-IPA(NH_2) due to the amino/nitro functional groups on their ligands (**Fig. S5a**). No impurity elements were detected, confirming the high purity of the synthesized materials. Subsequently, the Cu 2p spectra were further analyzed to determine the valence states of Cu (**Fig. 1e-f** and **S5b, c**). All Cu 2p spectra exhibited two main peaks corresponding to Cu $2p_{1/2}$ and Cu $2p_{3/2}$, along with distinct satellite peaks, which are typical features of Cu^{2+} species. Additionally, the Cu $2p_{3/2}$ region can be further resolved into two valence states: Cu^{2+} (~934–935 eV) and Cu^{+} (~932–933 eV), indicating the coexistence of mixed-valence copper species within the MOF frameworks. Quantitative analysis (Table S1) revealed that the Cu^{+}/Cu^{2+} ratio varies significantly with the organic ligand, with Cu-IPA exhibiting the highest value of 28.57%. This ligand-dependent variation in Cu^{+}/Cu^{2+} ratio correlates well with the catalytic activity trend observed in the PMS activation assays, wherein Cu-IPA also demonstrates the highest efficiency (**Fig. 2**). In addition, the isotherms obtained from gas adsorption experiments and the calculated surface areas are shown in **Fig. S6**. Among them, Cu-IPA exhibited the largest surface area (138.19 m^2/g), substantially exceeding those of Cu-PTA(NO_2) (11.53 m^2/g), Cu-PTA(NH_2) (26.48 m^2/g), Cu-IPA(NH_2) (9.82 m^2/g), and Cu-PTA (7.87 m^2/g). The superior surface area of Cu-IPA is also expected to contribute synergistically to its enhanced PMS activation performance.

Fig. 1

Performance Evaluation of Cu-MOFs for the Catalytic Activation of PMS

The PMS activation performance of the five Cu-MOFs was first evaluated using ABTS as the chromogenic substrate. As shown in **Fig. 2a-c** and **Fig. S7**, no distinct absorbance was observed in the absence of any single component (Cu-MOFs+ABTS,

Cu-MOFs+PMS, or ABTS+PMS), whereas the complete Cu-MOFs/PMS/ABTS system developed a characteristic absorption peak at 418 nm within 10 min, confirming that all five Cu-MOFs are capable of activating PMS to oxidize ABTS. To identify the most suitable chromogenic substrate for subsequent array construction, we compared ABTS, 3,3',5,5'-tetramethylbenzidine (TMB), and o-phenylenediamine (OPD) under identical conditions. As shown in **Fig. S8**, ABTS yielded the most differentiated responses among the five Cu-MOFs, whereas OPD showed nearly uniform activity and TMB remained inactive. ABTS was selected as the optimal substrate for subsequent sensor array construction. The reaction parameters were further optimized, revealing that maximum activity was achieved at 10 min, 25 °C, and pH 7.4 (**Fig. 2d-f**), which were adopted as the standard conditions for all subsequent sensing experiments.

Fig. 2

Under the optimized conditions, the PMS-activated ABTS oxidation activity of the five Cu-MOFs, as monitored by the absorbance at 418 nm, followed the order: Cu-IPA > Cu-PTA(NO_2) > Cu-PTA(NH_2) > Cu-IPA(NH_2) > Cu-PTA (**Fig. S9a**). To elucidate the origin of this catalytic activity, we performed control experiments with the corresponding free ligands and Cu^{2+} ions. As shown in **Fig. S9b**, none of the free ligands exhibited any detectable catalytic activity, confirming that the metal centers are the essential active sites for PMS activation. While free Cu^{2+} ions could indeed catalyze the oxidation of ABTS in the presence of PMS (**Fig. S9c**), their catalytic efficiency was substantially inferior to that of the Cu-MOFs, highlighting that the ordered metal-organic framework architecture significantly enhances the intrinsic activity of copper centers. Mechanistically, the activity order closely mirrors the Cu^{+}/Cu^{2+} ratio determined by XPS (**Table S1**). Cu-IPA, with the highest Cu^{+} content (28.57%), outperforms the other MOFs, suggesting that Cu^{+} is the predominant active species. The superior electron-donating ability of Cu^{+} likely promotes the reductive cleavage of PMS, accelerating the production of oxidative radicals that drive ABTS oxidation [16, 29]. Besides, the Cu^{+}/Cu^{2+} ratio of the aminated sample Cu-IPA (NH_2) is lower than that of the non-aminated Cu-IPA. This is likely due to the formation of stronger coordination bonds between the amino group and the copper center. As a two-electron

donor, the amino group forms a stable coordination bond with Cu^{2+} via the lone pair of electrons on the nitrogen atom, altering the electronic environment of the copper center and thereby reducing the relative content of Cu^{+}. In the TPA system, however, the Cu^{+}/Cu^{2+} ratio of Cu-TPA(NH_2) is higher than that of Cu-TPA. This may be because steric hindrance or electronic effects from the ligand backbone weaken the coordination strength between the amino group and copper, allowing the electron-donating effect of the amino group to dominate and thereby promoting the formation of Cu^{+}. The Cu^{+}/Cu^{2+} ratio in Cu-TPA(NO_2) is higher than that in Cu-TPA. This may be because the electron-withdrawing effect of the nitro group in this system actually helps increase the relative content of Cu^{+}, thereby enhancing catalytic activity.

In addition, to investigate the mechanism of catalytic activation of PMS, EPR spin-trapping techniques were employed to identify reactive oxide species (ROSs) in the Cu-IPA/PMS system. The generated ROSs were trapped using 5,5-dimethylpyrrolidine (DMPO) and 2,2,6,6-tetramethylpiperidine (TEMP). A clear 1:2:2:1 intensity ratio of the characteristic four peaks was observed (**Fig. S10a**). As time progressed, the peak intensities gradually increased, attributed to the generation of •OH during the activation of PMS. However, according to the literature[30, 31], the formation of DMPO-•OH depends on the nucleophilic addition of DMPO-SO_4•$^{-}$, rather than the direct capture of the •OH radical. To demonstrate the generation of SO_4•$^{-}$ in the Cu-IPA/PMS system, we added DMSO, a typical •OH quencher, to serve as an indicator of SO_4•$^{-}$. As shown in the **Fig. S10b**, the addition of DMSO resulted in the formation of DMPO-•CH_3 and an increase in DMPO-•OH, these two signals serve as reliable indicators of the presence of SO_4•$^{-}$. Furthermore, the six-peak pattern of O_2•$^{-}$ in **Fig. S10c** indicates the presence of O_2•$^{-}$ in the system. As shown in **Fig. S10d**, the intensity ratio of the 1:1:1 triple characteristic peak was clearly observed; this is attributed to the formation of TEMP-$^1O_2$ upon the reaction of TEMP with O_2. Similarly, the peak intensity gradually increased over time, further confirming the generation of $^1O_2$ in the oxidation system.

Construction of a Colorimetric Sensor Array for the Detection of AGs

To maximize the sensing sensitivity, three Cu-MOFs with higher activity (Cu-TPA(NO_2), Cu-TPA(NH_2), and Cu-IPA) were selected as the sensing channels. Their

distinct organic linkers provide differential binding affinities toward AGs, ensuring cross-reactive responses and high discrimination accuracy. Upon addition of 10 μg/mL AGs, the absorbance at 418 nm of each Cu-MOF/PMS/ABTS system shifted distinctively (**Fig. S12**), enabling the construction of a three-channel colorimetric array for five AGs (kanamycin (KAN), amikacin (AMK), tobramycin (TOB), gentamicin (GMC), and streptomycin (STR), structures in **Fig. S11**). Kinetic studies using Cu-IPA as a representative further confirmed that all five AGs could be rapidly identified within 5 min (**Fig. S13**).

To quantitatively characterize the differential responses, the inhibition rate, defined as $(A-A_0)/A_0$) (where A and A_0 are the absorbances with and without AGs, respectively), was calculated for each of the three sensing channels and presented as bar charts (**Fig. 3a**). As shown in the fingerprint-like response patterns, the five AGs exerted distinctly different modulatory effects on the PMS activation activity of the three Cu-MOFs. Specifically, KAN, AMK, and TOB enhanced the colorimetric signal, whereas STR suppressed it, and GMC exhibited a moderate effect. This differential behavior is primarily attributed to the structural and functional group variations among AGs, which govern their interaction modes with the MOF surfaces, including electrostatic interactions, hydrogen bonding, and π-π stacking [11, 32]. Depending on the nature of these interactions, the accessibility of the ABTS substrate to the catalytically active Cu sites may be either promoted or hindered, leading to enhancement or inhibition of the colorimetric response. Importantly, each AG also produced distinct response patterns across the three Cu-MOF channels. This cross-reactive diversity arises from the different physicochemical properties of the three MOFs, which collectively influence their PMS activation pathways and their recognition affinities toward different AGs. The resulting fingerprint spectra (**Fig. 3a**) serve as the unique signature for each AG, enabling reliable discrimination through subsequent LDA (**Fig. 3b**) and HCA analysis (**Fig. 3c**). As shown in the two-dimensional plot, the circles representing the confidence intervals for each of the five independent groups are mutually exclusive and do not overlap, indicating that this method can clearly distinguish AGs. The heatmap generated based on the inhibition

rates of each group exhibits distinct color anomalies, indicating significant differences between groups. Different antibiotics can be visually distinguished (**Fig. 3d**).

Fig. 3

Quantitative Analysis of AGs

Given that the concentration and composition of AGs in real-world samples are typically unknown, we systematically evaluated the quantitative and discriminative capabilities of the sensor array under more complex conditions. First, the five AGs were tested sequentially at six different concentrations (1, 3, 5, 7, 10, and 50 μg/mL) to establish the concentration-response relationship. As shown in **Fig. 4**, Factor 1 derived from LDA exhibited an excellent linear correlation with AG concentration over the range of 1-10 μg/mL, with coefficients of determination (R^2) exceeding 0.95 for all five antibiotics. This confirmed the feasibility of quantitative analysis using the proposed array. The corresponding heatmaps and HCA dendrograms further validated that each AG could be clearly distinguished across different concentration levels, demonstrating the array's robust qualitative and quantitative performance. To assess the practical utility of the sensor array for unknown sample identification, blind samples containing a single AG at a known concentration (10 μg/mL) but unknown identity were analyzed. By comparing the three-channel response patterns of each unknown sample with the established fingerprint library and LDA training model, all blind samples were correctly assigned to their respective AG categories (**Table S2**), achieving 100% classification accuracy. This result confirmed the reliability of the sensor array for accurate identification of unknown AGs at defined concentrations.

Considering that multiple antibiotics often coexist in real samples, we further challenged the sensor array with binary and ternary AG mixtures. A binary mixture of KAN and STR (total concentration of 10 μg/mL) was tested at various mass ratios (KAN/STR = 0%:100%, 30%:70%, 40%:60%, 60%:40%, 70%:30%, and 100%:0%). As shown in **Fig. S14a-c**, all mixture groups were clearly separated without any misclassification. Similarly, ternary mixtures of AMK, TOB, and GMC at different ratios were also well distinguished (**Fig. S14d-f**), with the three pure antibiotics located at the vertices of a triangular distribution and the mixtures positioned along the edges. .

These results demonstrate that the developed sensor array not only enables accurate identification of individual AGs but also exhibits excellent discriminatory power for complex mixtures, highlighting its potential for practical applications where multicomponent coexistence is common.

Fig. 4

Noise Immunity and Actual Sample Testing

Interference resistance is one of the most critical characteristics of a sensor, as the environment surrounding the sample being tested (typically an aqueous solution) is rarely pristine. 10 potential coexisting substances, including tetracycline, oxytetracycline, ciprofloxacin, NaCl, $MgSO_4$, K_2CO_3, lysine, urea, uric acid, and glucose were tested. As shown in the LDA plot (**Fig. 5a**), the five AGs (10 μg/mL, 5 replicates each) and the 10 interferents (10 μg/mL, 3 replicates each) formed clearly separated clusters without any overlap, indicating that the sensor array could reliably discriminate target antibiotics from diverse interfering species. HCA also revealed similar results (**Fig. 5b**). The entire analytical system was first divided into two clusters to separate the antibiotics from the interferents, and then progressively clustered into five distinct groups. This validated the sensor array's exceptional tolerance to diverse interferences.

The practical applicability of the sensor array was further validated by analyzing commercially available gentamicin sulfate and bismuth subnitrate capsules. In the experiment, the active ingredient was extracted from the capsules and prepared into solutions of varying concentrations. First, a 10 μg/mL sample was used for qualitative analysis and compared with the standard fingerprint and LDA patterns of aminoglycoside antibiotics at 10 μg/mL to verify that the sample was indeed gentamicin and that it could be clearly distinguished from other AGs (**Fig. 5c**). Subsequently, samples of varying concentrations were introduced, and a similar experimental procedure was followed. Through LDA and HCA pattern analysis, the five types of gentamicin samples were successfully classified with high clarity (**Fig. 5d, e**). Furthermore, a confusion matrix was constructed to evaluate the classification accuracy of the sensor array. As shown in **Fig. 5f**, the predicted labels perfectly matched the true

labels across all concentration groups, achieving 100% classification accuracy (Wilks' $\Lambda = 0.006$, $\chi^2 = 51.761$, $P < 0.001$). These results collectively demonstrate that the developed sensor array exhibits reliable performance in real-sample analysis and holds significant promise for practical applications in aminoglycoside antibiotic monitoring.

Fig. 5

Conclusions

In summary, we have developed a ligand-microenvironment-engineered Cu-MOF-based three-channel colorimetric sensor array for the rapid and accurate discrimination of five aminoglycoside antibiotics. The key innovation lies in the first-time introduction of PMS as a catalytic mediator for AGs sensing, which combined with the rational screening of three Cu-MOFs (Cu-TPA(NO_2), Cu-TPA(NH_2), and Cu-IPA) through simple ligand modulation, tailors their Cu^+/Cu^{2+} ratios and PMS activation efficiencies, yielding distinct cross-reactive responses toward structurally similar AGs. Coupled with machine learning algorithms (LDA and HCA), the array enables qualitative identification and quantitative analysis within 5 min, overcoming the concentration-dependent misclassification that plagues conventional single-material sensors. The successful discrimination of AG mixtures and reliable performance in commercial drug samples underscore its practical utility. This work not only expands the application scope of Cu-MOF nanozymes in antibiotic sensing but also establishes a generalizable paradigm for PMS-mediated rapid catalytic sensor arrays with potential for extension to other classes of environmental pollutants and pharmaceutical residues.

CRediT authorship contribution statement

Zhiyuan Luo: Investigation, Data curation, Writing-original draft. **Ziyi Zhao:** Validation, Investigation. **Hailong Shi:** Validation, Investigation. **Lingyun Chen:** Investigation. **Miao Zhang**: Data curation. **Haixia Feng**: Data curation. **Yuwan Lu:** Writing – review & editing, Project administration**. Siqi Li:** Conceptualization, Supervision, Writing – review & editing, Project administration.

Competing interests

The authors declare no competing interests.

Declaration of generative AI and AI-assisted technologies in the writing process

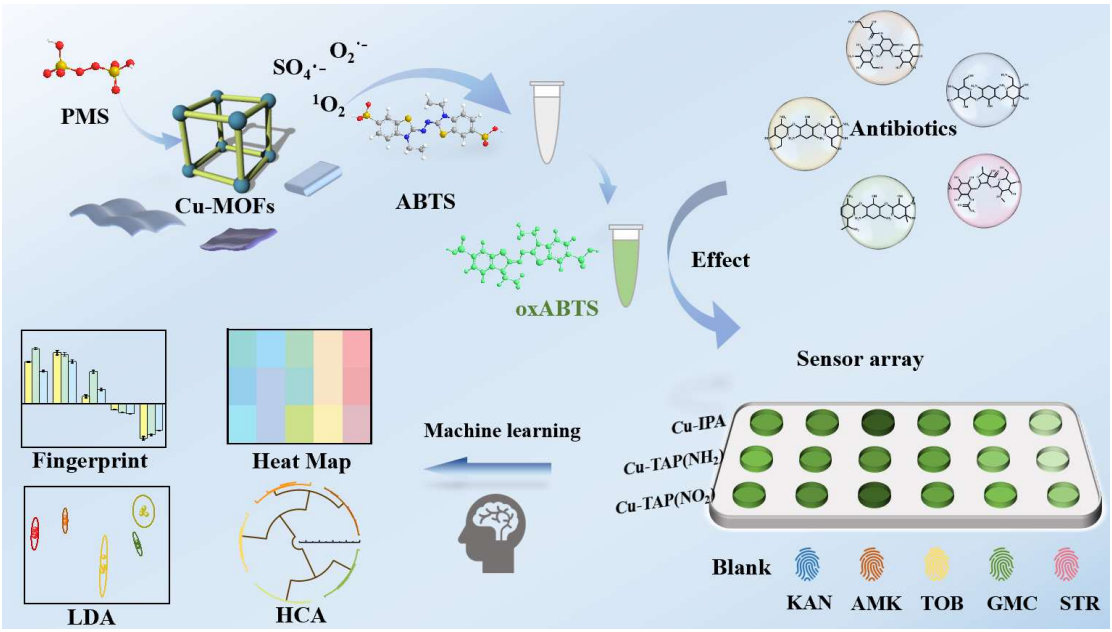
During the preparation of this work, the authors used ChatGPT in order to improve language. After using this tool, the authors reviewed and edited the content as needed and take full responsibility for the content of the publication.

Funding

This work was financially supported by the National Natural Science Foundation of China (No. 22506012; 22206018); Science and Technology Research Program of Chongqing Municipal Education Commission (No. KJZD-K202401106); Research Foundation of Chongqing University of Science and Technology (No. ckrc20241213); High Quality Development Plan for Graduate Education Foundation of Chongqing University of Technology (No. CYS240723).

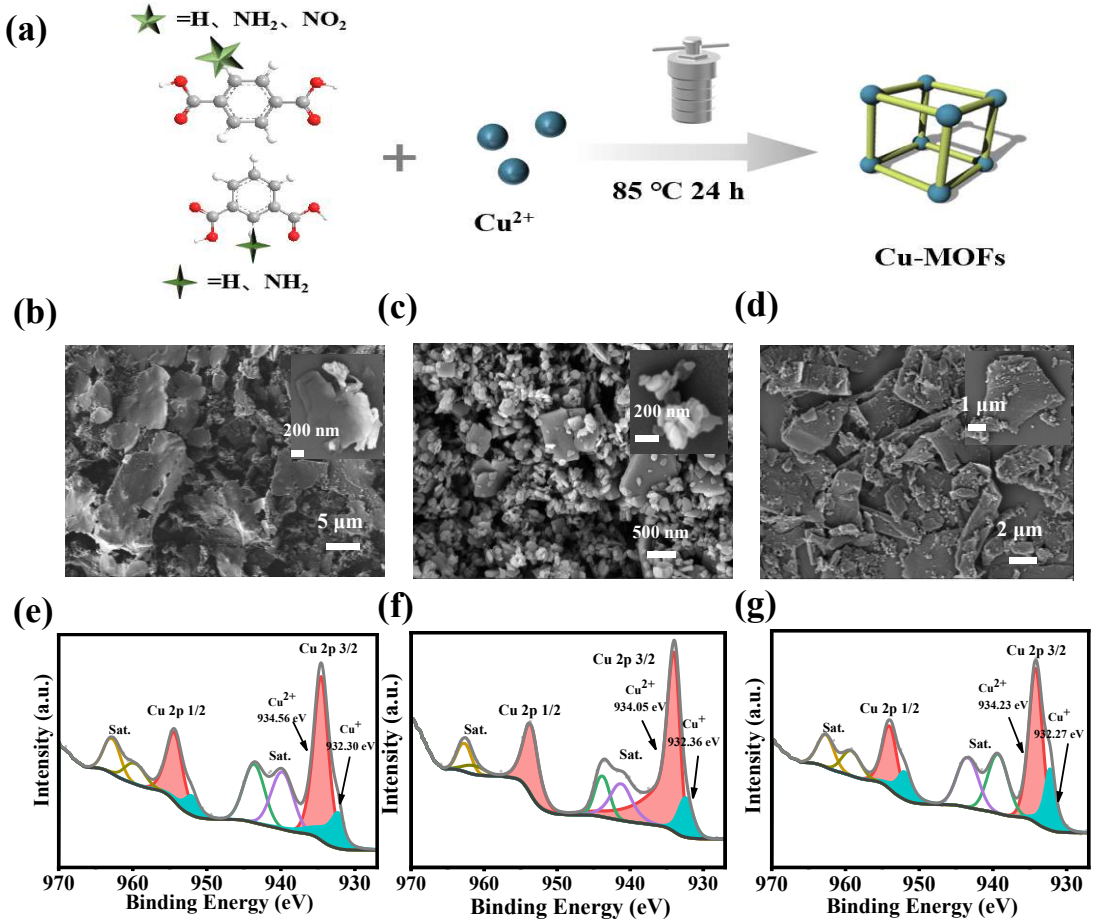
Supplementary materials

Supplementary material associated with this article can be found in the online version at doi:



405

406 **Scheme 1** Sensor Array Based on Cu-MOFs for Detecting AGs.

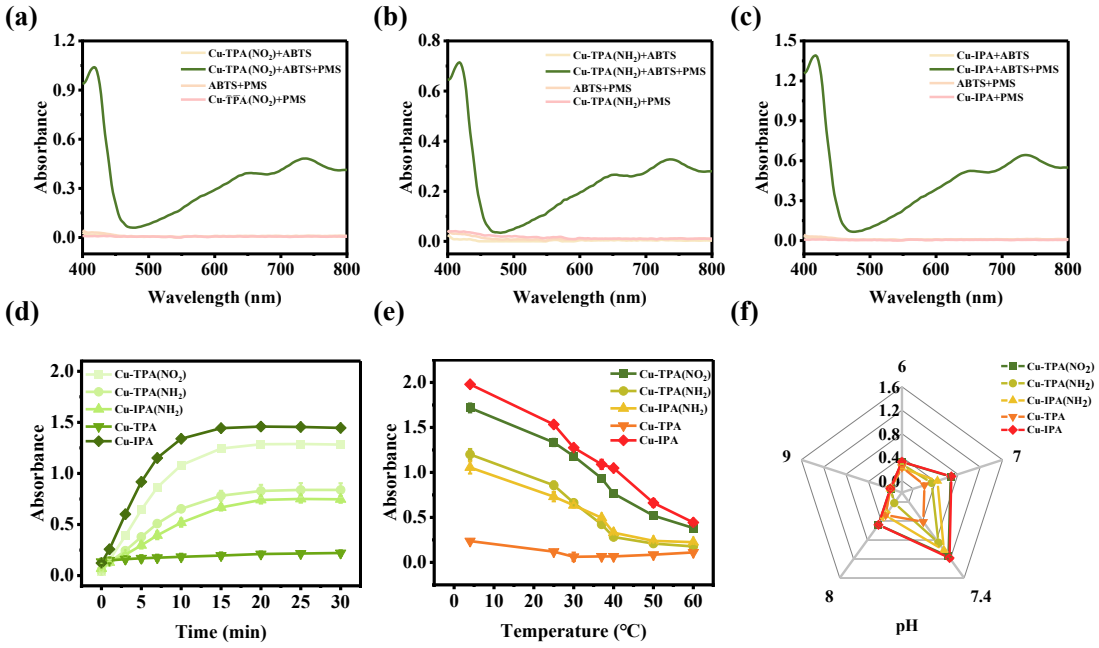


407

408 **Fig. 1** (a) Schematic diagram of Cu-MOF synthesis. SEM images of Cu-TPA(NO_2) (b),

409 Cu-TPA(NH_2) (c) and Cu-IPA (d). XPS spectra of Cu-TPA(NO_2) (e), Cu-TPA(NH_2) (f)

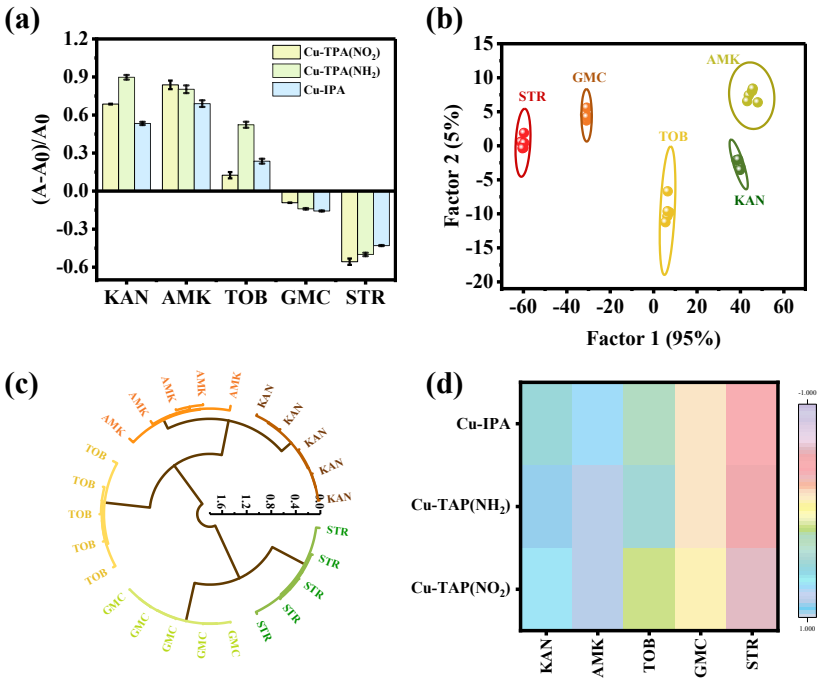
410 and Cu-IPA(g).



411

412 **Fig. 2** UV absorption spectra of Cu-TPA(NO_2) (a), Cu-TPA(NH_2) (b) and Cu-IPA(c)
413 in different systems, Comparison of PMS activation capabilities among five Cu-MOFs
414 under different time (d), temperature (e), and pH (f).

415



416

417 **Fig. 3** Fingerprint profiles (a), LDA score plots (b), circular dendrograms (c), and
418 heatmaps (d) reveal the characteristics of five different aminoglycoside antibiotics at a
419 concentration of 10 μg/mL.

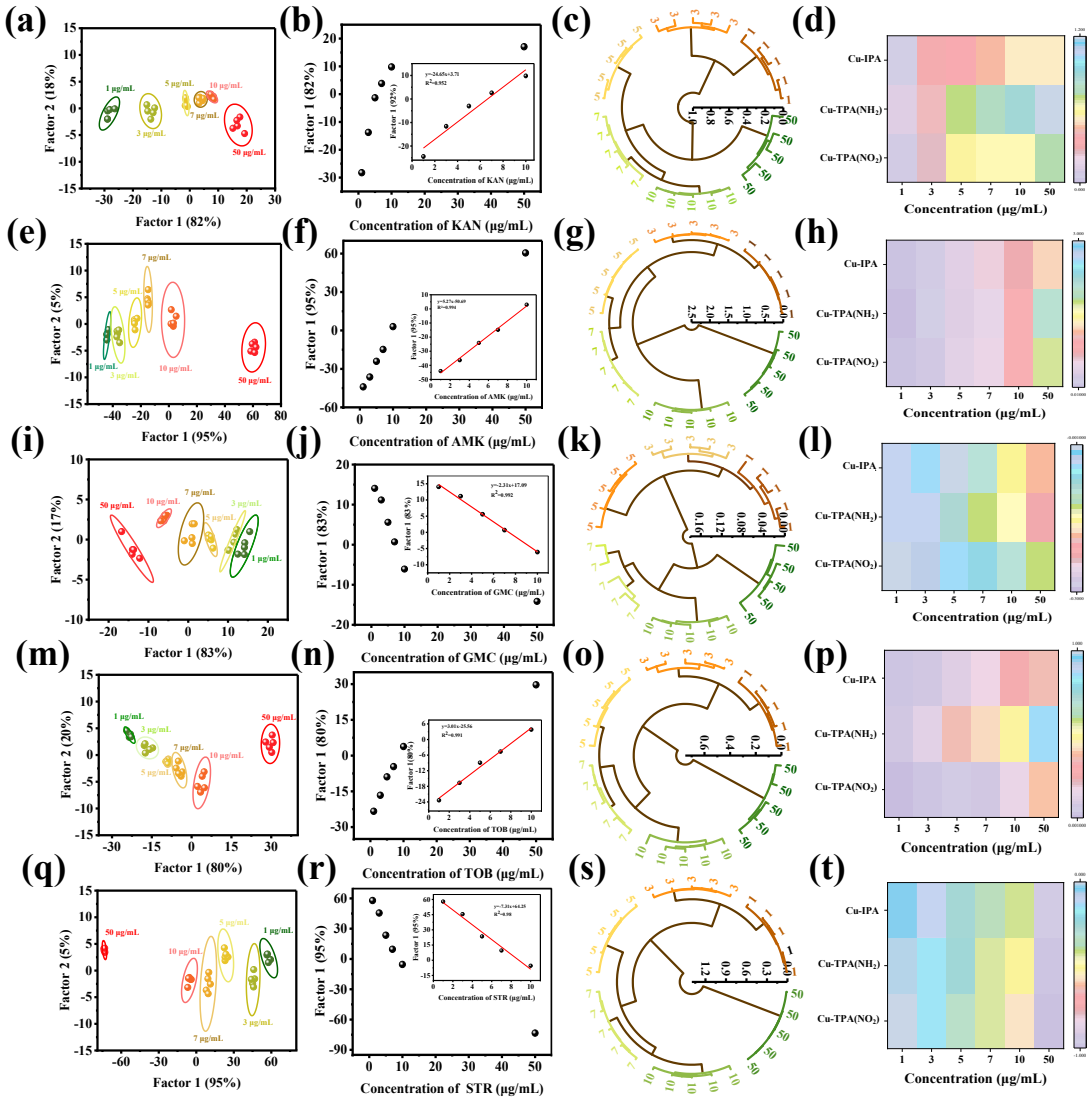


Fig. 4 LDA score plot, linear fit between Factor 1 and concentration, hierarchical cluster analysis (HCA) circular dendrogram, and heatmap, corresponding to kanamycin (a–d), amikacin (e–h), Tobramycin (i–l), Gentamicin (m–p), and Streptomycin (q–t), with a concentration range of 1−50 μg/mL.

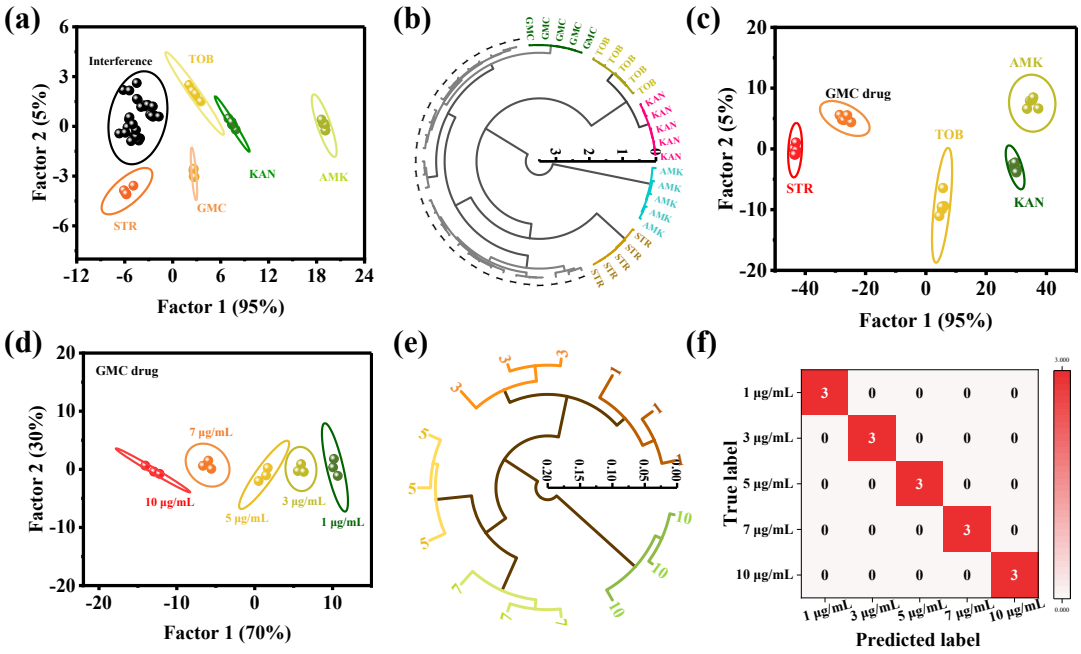


Fig. 5 Sensor array interference detection for five aminoglycoside antibiotics and ten interfering compounds, along with corresponding LDA score plots (a) and HCA ring clustering diagrams (b). LDA score plot (c), HCA circular clustering diagram (d), heatmap (e), and confusion matrix (f) for concentration identification results of purchased gentamicin sulfate and bismuth subnitrate capsules.

Reference

[1] Garneau-Tsodikova S, Labby K J (2016) Mechanisms of resistance to aminoglycoside antibiotics: overview and perspectives, Medchemcomm 7: 11-27. https://doi.org/10.1039/c5md00344j.

[2] Panda A, Halder K, Debnath D, De S M Y, DasguTPA S (2023) Thermodynamics of the association of aminoglycoside antibiotics with human angiogenin, Protein and Peptide Letters 30: 92-101. https://doi.org/10.2174/0929866530666221021111823.

[3] Kahlmeter G, Dahlager J I J J O a C (1984) Aminoglycoside toxicity–a review of clinical studies published between 1975 and 1982, J Antimicrob Chemother 13: 9-22. https://doi.org/10.1093/jac/13.suppl_A.9.

[4] Gao Z, Cheng Y, Long C, Tang W, Liu Q, Chen X (2025) Dual-nanozyme cascade for system-wide specific colorimetric detection of aminoglycoside antibiotics, Analytical Chemistry 97: 6136-6144. https://doi.org/10.1021/acs.analchem.4c06854.

[5] Luo Y T, Sun Y W, Wei X X, He Y Y, Wang H X, Cui Z W, Ma J Q, Liu X C, Shu R X, Lin H Q, Xu D P (2024) Detection methods for antibiotics in wastewater: A review, Bioprocess and Biosystems Engineering 47: 1433-1451. https://doi.org/10.1007/s00449-024-03033-0.

[6] Nian Q, Yang H, Meng E, Wang C, Xu Q, Zhang Q J C (2023) Efficient adsorptive removal of aminoglycoside antibiotics from environmental water, Chemosphere 337: 139379. https://doi.org/10.1016/j.chemosphere.2023.139379.

[7] Ema F A, Shanta R N, Rahman M Z, Islam M A, Khatun M M (2022) Isolation, identification, and antibiogram studies of Escherichia coli from ready-to-eat foods in Mymensingh, Bangladesh, Veterinary World 15: 1497-1505. https://doi.org/10.14202/vetworld.2022.1497-1505.

[8] Shan J R, Yin X C, Liu S J, Gong W J, Bai Y Y, Du T, Sun J, Zhang D H, Gu Y, Wang J L (2024) Defect-engineering-induced vacancy-rich Bi_2S_3-x@AuNPs with enhanced photothermal activity for sensitive bimodal-type gentamicin monitoring, Analytical Chemistry 96: 18564-18573. https://doi.org/10.1021/acs.analchem.4c05023.

[9] Foudraine D E, Dekker L J M, Strepis N, Nispeling S J, Raaphorst M N, Kloezen W, Colle P, Verbon A, Klaassen C H W, Luider T M, Goessens W H F (2022) Using

targeted liquid chromatography-tandem mass spectrometry to rapidly detect β-lactam, Aminoglycoside, and fluoroquinolone resistance mechanisms in blood cultures growing E. coli or K. pneumoniae, Frontiers in Microbiology 13. https://doi.org/10.3389/fmicb.2022.887420.

[10] Tan L, Li Y L, Wu X T, Liu W Q, Peng Z H, Dong Y S, Huang Z Y, Zhang L, Liang Y (2023) Fluorescent sensor array based on Janus silica nanoflakes to realize pattern recognition of multiple aminoglycoside antibiotics and heavy metal ions, Sensors and Actuators B-Chemical 378. https://doi.org/10.1016/j.snb.2022.133154.

[11] Zhen L, Li J, Bi Z, Zhang X, Jin P, Huang H, Li Y (2025) A three-channel nanozyme sensor array combined with machine learning algorithm for the differentiation and detection of aminoglycoside antibiotics, Chemical Engineering Journal 522. https://doi.org/10.1016/j.cej.2025.167711.

[12] Liang L, Yang R T, Wu J, Qin Y, Jiang Y T, Zhao S L, Ye F G (2024) Analyte-induced specific regulation of light-responsive COF-Cu nanozyme activity for ultrafast thiram colorimetric sensing, Analytical Chemistry 96: 18545-18554. https://doi.org/10.1021/acs.analchem.4c04534.

[13] Ma Y F, Li Y W, Ma K, Wang Z (2018) Optical colorimetric sensor arrays for chemical and biological analysis, Science China-Chemistry 61: 643-655. https://doi.org/10.1007/s11426-017-9224-3.

[14] Chen Z H, Fan Q X, Han X Y, Shi G Y, Zhang M (2020) Design of smart chemical 'tongue' sensor arrays for pattern-recognition-based biochemical sensing applications, Trac-Trends in Analytical Chemistry 124. https://doi.org/10.1016/j.trac.2019.115794.

[15] Huang Y, Liu T, Xiong Y, Wen Q, Li W, Ren J, Zhong H (2025) A three-channel colorimetric sensor array utilizing various Fe-MOFs for simultaneous discrimination of multiple pesticides, Food Chemistry 496. https://doi.org/10.1016/j.foodchem.2025.146895.

[16] Shen X, Ma S, Song C, He Y, Li M (2025) Kinetic and Mechanistic Discrepancies of Single/Dual-Atom Nanozymes Drive a Triple-Channel Sensing Array for Machine Learning-Assisted Antioxidant Discrimination, Analytical Chemistry 97: 19957-19970. https://doi.org/10.1021/acs.analchem.5c04478.

[17] Wei D L, Zhang H, Tao Y, Wang K X, Wang Y, Deng C M, Xu R F, Zhu N F, Lu Y Y, Zeng K, Yang Z G, Zhang Z (2024) Dual-Emission Single Sensing Element-Assembled Fluorescent Sensor Arrays for the Rapid Discrimination of Multiple Surfactants in Environments, Analytical Chemistry 96: 4987-4996. https://doi.org/10.1021/acs.analchem.4c00108.

[18] Zeng K, Wang Y N, Tao Y, Huang R, Dong Q W, Deng C M, Wu Q Y, Niu X H, Wei D L, Zhang Z (2025) Single sensing element with multiple adsorption peaks assembled nanozyme sensor array for discrimination of multiple metal ions, Microchemical Journal 209. https://doi.org/10.1016/j.microc.2025.112786.

[19] Yang M, Zhai X D, Huang X W, Li Z H, Shi J Y, Li Q, Zou X B, Battino M (2021) Rapid discrimination of beer based on quantitative aroma determination using colorimetric sensor array, Food Chemistry 363. https://doi.org/10.1016/j.foodchem.2021.130297.

[20] Li L Q, Li M H, Cui Q Q, Liu Y, Chen Y Y, Wang Y J, Zhang Z Z, Chen Q S, Ning J M (2022) Rapid monitoring of black tea fermentation quality based on a solution-phase sensor array combined with UV-visible spectroscopy, Food Chemistry 377: 131974. https://doi.org/10.1016/j.foodchem.2021.131974.

[21] Xu L, Wang H, Xu Y, Cui W Y, Ni W W, Chen M Q, Huang H, Stewart C, Li L X, Li F, Han J S (2022) Machine learning-assisted sensor array based on poly(amidoamine) (PAMAM) dendrimers for diagnosing Alzheimer's Disease, ACS Sensors 7: 1315-1322. https://doi.org/10.1021/acssensors.2c00132.

[22] Li H Y, Wang X, Chen Y F, Leng H, Bai J J, Lu Y, Wang N, Du C, Wang J H, Chen M L (2025) Lanthanide-assisted function tailoring of the HOF-based logic gate sensor array for biothiol detection and disease discrimination, Analytical Chemistry 97: 1758-1766. https://doi.org/10.1021/acs.analchem.4c05296.

[23] Zhu X Y, Li T, Hai X, Bi S (2022) A nanozyme-based colorimetric sensor array as electronic tongue for thiols discrimination and disease identification, Biosensors & Bioelectronics 213: 114438. https://doi.org/10.1016/j.bios.2022.114438.

[24] Yin J H, Liu M X, Lan C W, Chu B Q, Meng L, Xu N (2023) Catechol oxidase nanozyme based colorimetric sensors array for highly selective distinction among

multiple catecholamines, Analytica Chimica Acta 1279: 341823. https://doi.org/10.1016/j.aca.2023.341823.

[25] Li Y Y, Mu Z D, Yuan Y H, Zhou J, Bai L J, Qing M (2023) An enzymatic activity regulation-based clusterzyme sensor array for high-throughput identification of heavy metal ions, Journal of Hazardous Materials 454. https://doi.org/10.1016/j.jhazmat.2023.131501.

[26] Jing W J, Yang Y J, Shi Q H, Wang Y, Liu F F (2024) Machine learning-based nanozyme sensor array as an electronic tongue for the discrimination of endogenous phenolic compounds in food, Analytical Chemistry 96: 16027-16035. https://doi.org/10.1021/acs.analchem.4c03586.

[27] Wei D, Li M, Yang Y, Deng C, Zhu F, Li M, Deng Y, Zhang Z (2025) Ligand microenvironment-regulated nanozymes enabled machine learning-assisted sensor array for simultaneous identification of phenolic pollutants, ACS Sensors 10: 5245-5255. https://doi.org/10.1021/acssensors.5c01499.

[28] Song D, Tian T, Wang L, Zou Y, Zhao L, Xiao J, Huang H, Li Y (2024) Multi-signal sensor array based on a fluorescent nanozyme for broad-spectrum screening of pesticides, Chemical Engineering Journal 482: 148784. https://doi.org/10.1016/j.cej.2024.148784.

[29] Zeng X L, Wang H R, Ma Y T, Xu X, Lu X X, Hu Y J, Xie J H, Wang X, Wang Y S, Guo X L, Zhao L, Li J C (2023) Vanadium oxide nanozymes with multiple enzyme-mimic activities for tumor catalytic therapy, ACS Applied Materials & Interfaces 15: 13941-13955. https://doi.org/10.1021/acsami.2c20878.

[30] Bai S, Wang P, Xu C, Wang L, Hu X, Hu P, Fu Y, Wang Z (2026) Dimethyl sulfoxide as a qualitative EPR indicator of sulfate radical in advanced oxidation processes, Water Research 289. https://doi.org/10.1016/j.watres.2025.125011.

[31] Chen L, Duan J, Du P, Sun W, Lai B, Liu W (2022) Accurate identification of radicals by in-situ electron paramagnetic resonance in ultraviolet-based homogenous advanced oxidation processes, Water Research 221. https://doi.org/10.1016/j.watres.2022.118747.

[32] Wei D L, Zhang X Y, Chen B, Zeng K (2020) Using bimetallic Au@Pt nanozymes

as a visual tag and as an enzyme mimic in enhanced sensitive lateral-flow immunoassays: Application for the detection of streptomycin, Analytica Chimica Acta 1126: 106-113. https://doi.org/10.1016/j.aca.2020.06.009.

Supplementary Files

This is a list of supplementary files associated with this preprint. Click to download.

- 2026.8.SupportingInformation.docx